Materials Science & Engineering A 935 (2025) 148392

Contents lists available at ScienceDirect

Materials Science & Engineering A

journal homepage: www.elsevier.com/locate/msea

Toughening nitride hard coatings by deflecting cracks along grain boundaries

Yinxia Zhang [a], Matthias Bartosik [b], Steffen Brinckmann [c], Subin Lee [a,*], Christoph Kirchlechner [a]

[a] Institute for Applied Materials, Karlsruhe Institute of Technology, D-76131, Karlsruhe, Germany
[b] Department of Materials Science, Montanuniversität Leoben, A-8700, Leoben, Austria
[c] Microstructure and Properties of Materials (IMD-1), Forschungszentrum Jülich GmbH, D-52428, Jülich, Germany

ARTICLE INFO

Keywords:
Crack deflection
Hard coatings
Toughening mechanism
Fracture toughness
Grain boundary fracture

ABSTRACT

Grain boundaries (GBs) in hard coatings are often considered as the weakest link, acting as preferred pathways for crack propagation and thereby limiting the coating's fracture toughness. In this study, we investigate whether continuous crack deflection along GBs can mitigate this limitation and enhance the fracture resistance of hard coatings. Three model systems were examined: CrN, AlN and their multilayered structure coatings, all characterized by columnar GB structures. Fracture toughness was quantitatively assessed using an *in situ* SEM microcantilever fracture testing. The key approach of this study is the use of two different loading geometries, with notches aligned either parallel or perpendicular to the coating's growth direction, allowing us to compare the influence of the crack propagation direction and deflection. Across all three systems, the perpendicular notch configuration—aligned across the columnar microstructure—resulted in approximately 8 % higher fracture toughness. This enhancement is attributed to continuous crack deflection along GBs during deformation. Additionally, the extent of crack deflection was found to depend on the local GB arrangement, with transgranular fracture observed when no well-aligned GBs were present along the crack path. These findings provide quantitative insights into the toughening mechanisms enabled by GB-mediated crack deflection and offer design strategies for mechanically robust hard coatings.

1. Introduction

Hard coatings, composed mainly of metal carbides or nitrides, are widely used in aerospace [1], automotive engineering [2], and cutting tools for manufacturing [3] due to their ability to extend component service life by providing protection against harsh environments [4–7]. A critical property of these coatings is their toughness, fundamentally represented by the fracture toughness, K_{IC} [8–12]. During fabrication—particularly in coatings synthesized using physical vapor deposition (PVD)—a columnar grain microstructure with elongated grains aligned parallel to the growth direction often forms [13–16]. Grain boundaries (GBs) have been reported to act as preferential pathways for crack propagation, thereby reducing fracture toughness. Consequently, due to their anisotropic microstructure with elongated columnar grains, PVD-grown hard coatings are expected to exhibit orientation-dependent fracture toughness, which varies with the crack propagation direction relative to the columnar microstructure's orientation, hereafter referred to as the GBs orientation.

However, quantifying the anisotropic fracture behavior poses significant challenges due to their micrometer-scale thickness and limited volume, requiring the use of fracture testing at the microscale [17–19]. Several studies have reported the effect of crack propagation direction on the fracture toughness of hard coatings using micromechanics [20–25], as well as the anisotropic nature of fracture toughness [24–27]. For instance, a nanostructured NbMoTaW high-entropy alloy thin film exhibited lower fracture toughness when tested perpendicular to the film growth direction compared to tests performed parallel to the growth direction [27]. In contrast, a recent study by Schoof et al. on vanadium-aluminum (oxy)nitride coatings revealed higher K_{IC} when tested perpendicular to the growth direction in coatings with a columnar grain structure [24]. These contrasting observations underscore the inconsistencies in the role of GB orientation in hard coatings which may

This article is part of a special issue entitled: Nanomechanical Testing 2024 published in Materials Science & Engineering A.

* Corresponding author.
E-mail address: subin.lee@kit.edu (S. Lee).

https://doi.org/10.1016/j.msea.2025.148392
Received 31 January 2025; Received in revised form 20 April 2025; Accepted 22 April 2025
Available online 23 April 2025

Table 1
Nomenclature and abbreviations used in the manuscript.

Abbreviation	Definition
CrN	Chromium nitride
AlN	Aluminum nitride
CrN/AlN multilayer	Multilayer structure composed of alternating CrN and AlN layers
PVD	Physical vapor deposition
GB	Grain boundary
SEM	Scanning electron microscope
FIB	Focused ion beam
∥-notch	A notch parallel to the coating growth direction
⊥-notch	A notch perpendicular to the coating growth direction

depend on the material and even specific GB properties. Moreover, while nitride coatings have been extensively studied, a quantitative analysis addressing the influence of GB orientation still remains lacking for CrN and AlN.

This study aims to explore the anisotropy in fracture toughness and crack propagation behavior of three nitride hard coatings—CrN, AlN, and their laminated structure—by focusing on the role of columnar microstructure and GBs. To this end, *in situ* scanning electron microscope (SEM) micro-cantilever bending tests were performed under two distinct loading directions: one promoting crack propagation parallel to the coating growth direction, and the other perpendicular to it, thereby altering the orientation of the crack path relative to the columnar grain structure. By employing the same coating system under two distinct loading directions, we were able to isolate and quantify the effect of GB orientation on fracture toughness, independent of other microstructural variations that may arise during synthesis. This approach eliminates confounding variables associated with comparing different coatings, enabling a direct assessment of how GB alignment and crack propagation direction influence fracture toughness.

Our results reveal that in all three coatings, cracks propagating perpendicular to the growth direction underwent continuous crack deflection along GBs due to smaller effective grain size encountered along their path, resulting approximately 8 % increase in fracture toughness. In contrast, when the crack propagated parallel to the columnar structure, the GBs were aligned with the crack path, allowing relatively smooth propagation and thus lower toughness. To the best of our knowledge, this is the first quantitative assessment of fracture toughness anisotropy in CrN and AlN coatings using micro-fracture testing. These findings not only demonstrate the critical role of GB orientation and crack deflection in enhancing fracture toughness, but also provide a valuable framework for microstructure-guided design of mechanically robust hard coatings.

2. Experimental procedures

Three different coatings were prepared using unbalanced reactive magnetron sputtering: (1) a monolithic CrN coating with a thickness of 1.5 μm on Si (100) substrates, (2) a 4.0 μm thick monolithic AlN coating on MgO (100) substrates, and (3) a CrN/AlN multilayer coating with a thickness of 1.9 μm on Si (100) substrates. The CrN/AlN multilayer coating consists of alternating layers of approximately 4 nm of CrN and 2 nm of AlN [28]. The phase of the films was analyzed using X-ray diffraction [29]. SEM (Merlin Gemini II, Zeiss) and focused ion beam (FIB) (Crossbeam 550L, Zeiss) were used to characterize the surface and cross-sectional microstructure of the samples. A list of abbreviations used for sample structures and testing methods is provided in Table 1.

CrN and AlN coatings were deposited on different substrates—Si and MgO, respectively—to introduce variations in substrate type, crystal structure (cubic for CrN vs. hexagonal for AlN), grain size, and residual stress. This allowed us to evaluate how these factors affect crack propagation along grain boundaries and overall fracture toughness. The CrN/AlN multilayer, deposited on the same substrate as CrN, shares the cubic structure but incorporates a nanoscale layered architecture, enabling the influence of multilayering and associated residual stress to be assessed.

The depositions were carried out in an AJA ATC-1800 ultra-high vacuum deposition system, equipped with Cr and Al targets, each with a three-inch diameter and 99.99 % purity. The targets were powered in pulsed DC mode at 100 kHz with a 1 μs pause. The Cr and Al targets were subjected to time-averaged powers of 300 W and 500 W, respectively. The coatings were grown in a gas mixture of N_2 at a flow rate of 12 sccm and Ar at a flow rate of 8 sccm, with a total gas pressure of 0.2 Pa. To obtain a dense coating morphology, a DC bias voltage of −70 V was applied to the substrates during coating growth. Throughout the deposition process, the deposition parameters were kept constant while computer-controlled mechanical shutters periodically opened and closed to create the multilayer structure of the CrN/AlN multilayer coating. During deposition, the substrates were constantly rotated with a frequency of about 0.5 Hz. More detailed information of the deposition processes can be found in Ref. [30].

Before fabricating micro-cantilevers, the Si substrates of CrN/AlN multilayer and CrN coatings were etched using a 30 wt% potassium hydroxide solution at 60 °C for 30 min to obtain 20 μm-long free-standing film segments. Cantilevers were then fabricated by using FIB milling with Ga ions at an acceleration voltage of 30 kV (Crossbeam 550L, Zeiss). The ion beam current was varied as follows: 15 nA for coarse milling, 3 nA, 700 pA, 300 pA for intermediate steps, and 50 pA for final milling. The cantilevers of the AlN coating on MgO—which cannot be similarly etched as Si—required removal of the substrate by Ga ion milling with the same series of milling currents as mentioned

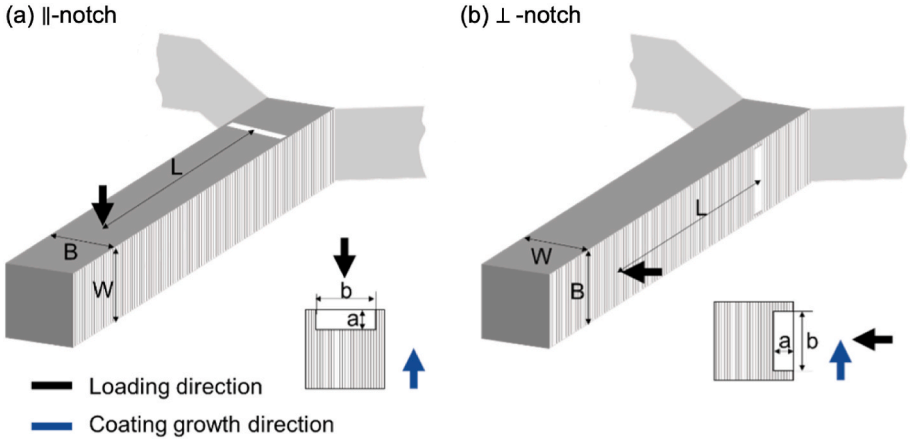

Fig. 1. Schematic illustration of two micro-cantilever geometries with different loading directions: (a) loading parallel to the coating growth direction (∥-notch), and (b) loading perpendicular to the growth direction (⊥-notch). The insets illustrate the cross-sectional view of the bridge notches.

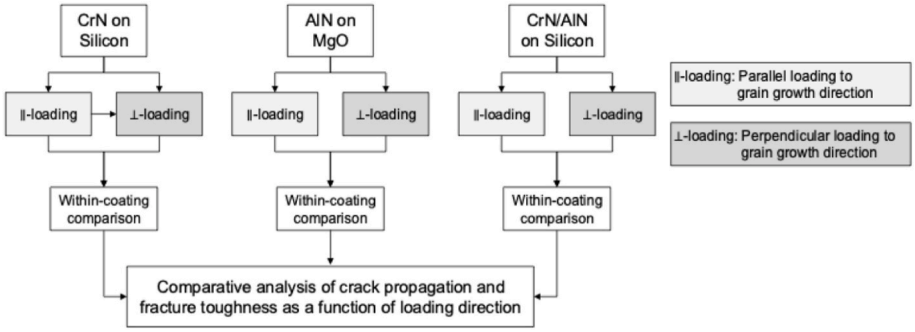

Fig. 2. Flowchart of the experimental design. Three coatings were tested under two loading directions (∥ and ⊥ to grain growth) to compare crack propagation behavior and K_{IC} values.

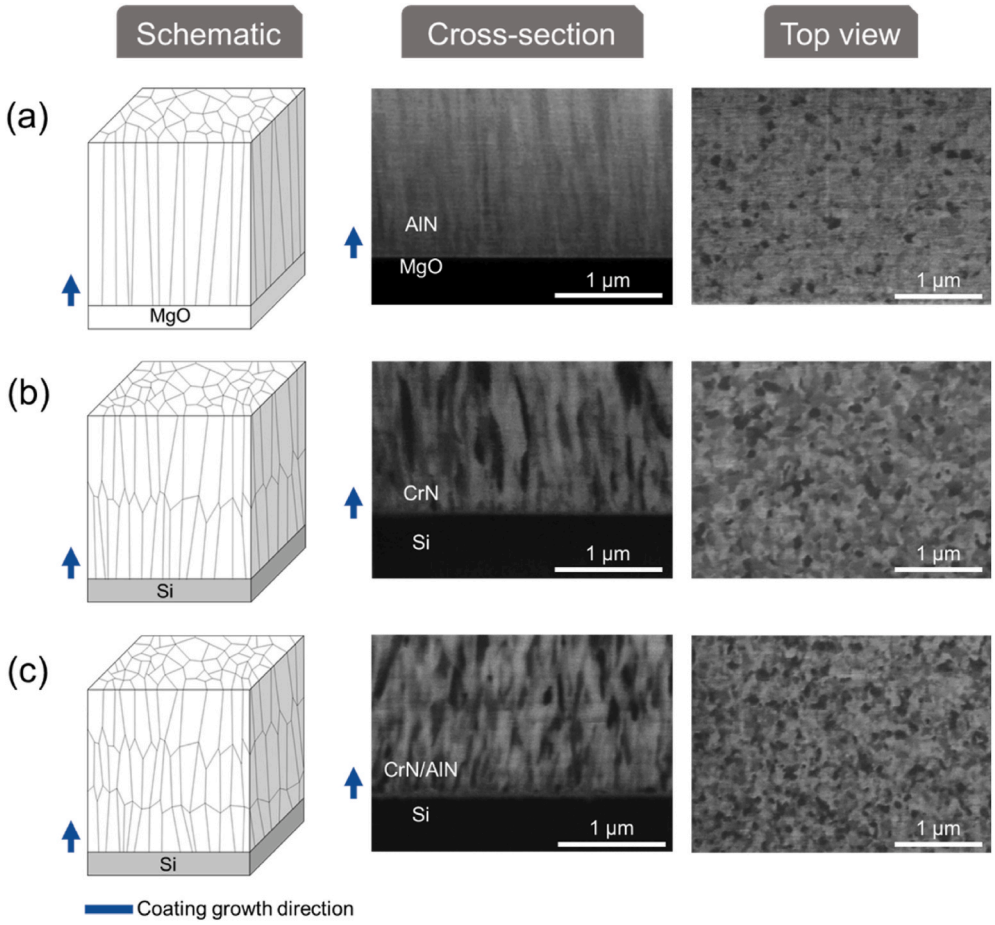

Fig. 3. The first column displays a schematic drawing of the microstructure, the second and the third columns are FIB channeling contrast images, showing the cross-section and the top view of each coating, (a) AlN on MgO, (b) CrN on Si, and (c) CrN/AlN on Si.

above. Notches were milled using a 20 pA current with a 1.0 μs dwell time. A bridge notch design retaining two ligaments on either side was employed instead of a straight through-thickness notch. The purpose of this design is to initiate a crack from the FIB-milled notch at the material bridge, and then arrest its propagation to form a naturally sharp crack, which triggers the final fracture of the cantilever [18,28]. The dimensions of the bridge notch cantilevers were prepared according to the schematic in Fig. 1, with L being the distance between the loading position and the notch, W is the thickness of the cantilever, B is the width of the cantilever, b is the width of the notch, and a is the depth of the notch. The thickness W varied from 1.5 μm to 2.5 μm, depending on the coating thickness (1.5 μm for the CrN coating, 1.9 μm for the CrN/AlN multilayer coating, and 2.5 μm for the AlN coating). To minimize geometry-related influences on the fracture response across samples with varying coating thicknesses, the L:W:B ratio was kept constant at 5:1:1 for all cantilevers by adjusting the width B accordingly. The notch depth, a, was set to 20–30 % of the cantilever thickness, and the bridge width was minimized to below 100 nm to enhance the stress concentration at the bridge, thereby promoting bridge failure and subsequent crack arrest [28].

Micromechanical fracture tests of the FIB-prepared cantilevers were conducted in an SEM with an *in situ* nanoindenter (Hysitron PI-89, Bruker) equipped with a 10 μm wide diamond wedge tip (Synton-MDP AG). All *in situ* SEM deformations were performed in a displacement-

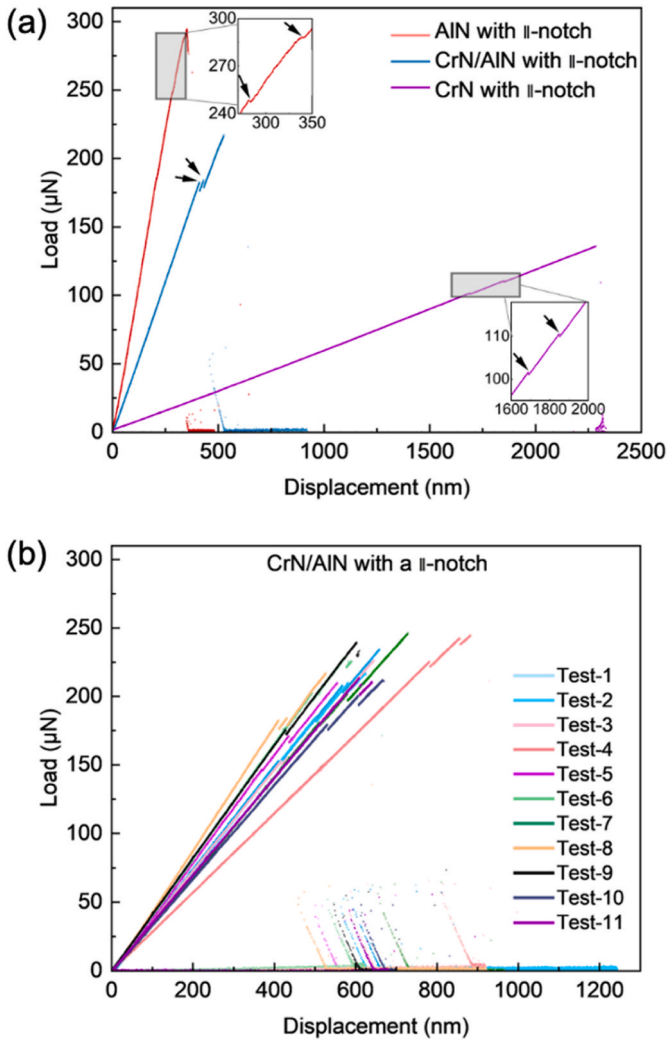

Fig. 4. (a) Load-displacement curves from a single test on AlN, CrN/AlN and CrN coatings with a ‖-notch. Arrows indicate the load drops caused by bridge failure and subsequent crack arrest. (b) All curves of 11 micro-cantilever fracture tests on CrN/AlN coating with a ‖-notch.

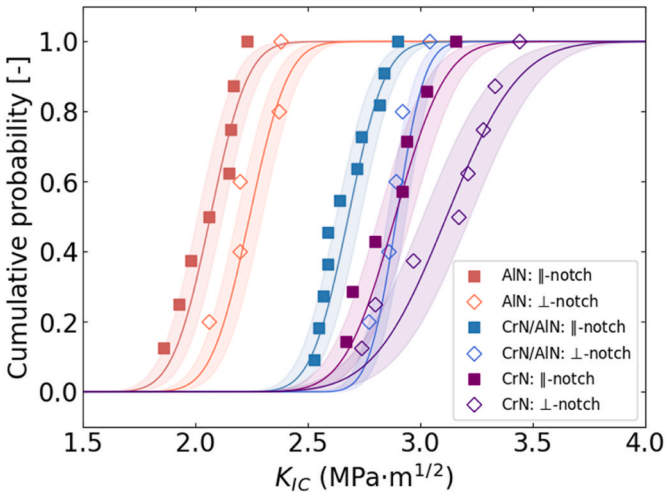

Fig. 5. Cumulative distribution of fracture toughness of AlN (red curves), CrN/AlN (purple curves), and CrN (blue curves) coatings. Data from ‖-notch cantilevers are represented by solid markers, while results from ⊥-notch cantilevers are indicated by open markers. (For interpretation of the references to colour in this figure legend, the reader is referred to the Web version of this article.)

controlled mode with a displacement rate of 5 nm/s. The maximum load of the transducer was 10 mN, and an intrinsic noise floor was 0.4 μN.

Indentation hardness was measured using a UMIS nanoindenter from Fischer-Cripps Laboratories. A diamond Berkovich tip was used, and the nanohardness and indentation modulus were calculated using the Oliver and Pharr method [31].

A schematic overview of the experimental procedure and comparative framework is provided in Fig. 2, illustrating the three different coating systems, the two loading directions, and the overall analysis logic.

3. Results and discussion

The microstructures of the three hard coatings investigated in this study are presented in Fig. 3. FIB channeling contrast imaging was performed on both the FIB cross-section and the top surface to analyze microstructure and grain size. The columnar grain structure, which is elongated along the film growth direction, is clearly revealed in all coatings. The columnar grains exhibit a grain size ranging from approximately 70 to 100 nm measured at the top surface.

Micro-cantilevers were fabricated using FIB to have two different crack propagation—and consequently load application—directions. In the first geometry, the crack propagation from the FIB-milled notch was parallel to the coating's growth direction, hereafter referred to as ‖-notch. In the second geometry, the crack propagation was perpendicular to the growth direction, and therefore perpendicular to the columnar grain direction, referred to as ⊥-notch. Please note that the global crack plane of both, the ‖- and the ⊥-notch, are identical, but only the crack propagation direction differ as the tests were performed on the same samples with different loading orientations. Therefore, crystallographic texture which typically is present in hard coatings does not cause the differences in the measured fracture toughness of samples with ‖- and the ⊥-notches.

Representative load–displacement curves from ‖-notched cantilevers are shown in Fig. 4(a), displaying the typical linear-elastic fracture of micro-cantilevers: a linear load increase up to a critical point, followed by sudden fracture [32,33]. Variations in the slopes of these curves, reflecting differences in sample stiffness, are primarily attributed to differences in sample geometry, such as film thickness. Load drops at the point of bridge failure, marked by black arrows and provided in a magnified view inside insets, indicate crack arrest similar to our previous report in Ref. [28]. These load drops occur because the thin material bridges on the cantilever body fail first due to localized stress concentration. This stress focusing at the bridge effectively arrests the crack temporarily and promotes fracture initiation from a naturally sharp crack tip formed during bridge failure [28]. A total of 8, 11, and 7 cantilevers with a ‖-notch were tested for AlN, CrN/AlN, and CrN coatings, respectively. All load-displacement curves for CrN/AlN coatings with ‖-notch are shown in Fig. 4(b) as examples. For comparison, the corresponding load-displacement curves for cantilevers with a ⊥-notch are provided in Fig. A.2 in the Supplementary Information. In all cases, the cantilevers failed in a brittle, linear-elastic fracture manner, exhibiting highly consistent load-displacement behavior across multiple specimens. Notably, in most cases, two distinct load drops were observed, indicating crack arrest due to bridge failure. This suggests that fracture initiated from a naturally sharp crack before final failure occurred [28].

The fracture toughness and failure characteristics of AlN, CrN/AlN, and CrN coatings were evaluated from the resulting load-displacement curves and the cantilever geometry. As shown in Fig. 4, all samples exhibited linear-elastic fracture with bridge failures, followed by final fracture at the arrested crack. Therefore, the fracture toughness, K_{IC}, calculated assuming a through-thickness notch geometry after crack arrest using the following equation [18]:

Table 2
Indentation hardness and Young's modulus of AlN, CrN/AlN, and CrN coatings. And their fracture toughness (MPa $m^{1/2}$) and standard error of the mean with ⊥- and ‖-notch.

Coating—Substrate	Hardness [GPa]	Young's modulus [GPa]	Fracture toughness (MPa $m^{1/2}$)	
			⊥-notch	‖-notch
AlN—MgO	20.3 ± 1.7	327 ± 20	2.24 ± 0.06	2.07 ± 0.05
CrN/AlN—Si	28.2 ± 0.7	314 ± 9	2.90 ± 0.04	2.68 ± 0.04
CrN—Si	21.7 ± 0.9	309 ± 10	3.12 ± 0.09	2.89 ± 0.07

$$K_{IC} = \frac{FL}{BW^{\frac{3}{2}}} f_{Matoy}\left(\frac{a}{W}\right) \quad (1)$$

$$f_{Matoy}\left(\frac{a}{W}\right) = 1.46 + 24.36(a/W) - 47.21(a/W)^2 + 75.18(a/W)^3 \quad (2)$$

where, F is the load at the final fracture, $f_{Matoy}\left(\frac{a}{W}\right)$ is a geometry shape factor, and L, B, W, and a are the parameters from the geometry of the cantilever.

The calculated fracture toughness, K_{IC}, of all cantilevers including those with ‖-notch or ⊥-notch, is plotted as a cumulative probability distribution for statistical analysis (Fig. 5). The data were fitted with a normal cumulative distribution function (CDF) where the 95 % confidence intervals are highlighted by shading. Firstly, we found that the AlN hard coating has a lower fracture toughness than the CrN hard coatings in both ⊥-notch and ‖-notch. The K_{IC} of the CrN/AlN multilayer coatings with a material volume ratio of 2 is in between the CrN and AlN coatings. The expected toughening effect from the nanoscale interfaces in the CrN/AlN multilayer was less pronounced, indicating that the interface density in the current design may not be sufficient to significantly enhance fracture resistance through crack deflection or energy dissipation mechanisms.

Additionally, in all three coatings, the cantilevers with ⊥-notch exhibited higher fracture toughness compared to those with ‖-notch (Fig. 5 and Table 2). An increase in fracture toughness of 8.4 %, 8.0 %, and 8.0 % was measured for AlN, CrN/AlN, and CrN micro-cantilevers, respectively, when ⊥-notch cantilevers were compared with ‖-notch cantilevers. These quantitative measurements highlight the critical role of GB orientation relative to the crack propagation direction in determining the fracture toughness of hard coatings, regardless of their chemical composition, or their substrate and resulting microstructural features such as grain size or residual stress.

Representative SEM images of the fracture surfaces on the tested micro-cantilevers are shown in Fig. 6. A columnar grain structure is observed in all SEM images, which is consistent throughout the coating's thickness. In the first row, where the crack propagation is parallel to the growth direction, the columnar microstructure is characterized by a vertically aligned pattern, while the fracture surfaces of the cantilevers with a ⊥-notch exhibit horizontal features in the second row. Fractography shows the crack propagation mainly along GBs regardless of notch orientation, indicating that intergranular fracture was the dominating fracture mechanism.

Crack propagation was further analyzed based on the fractured surface. In the case of ⊥-notches, cracks continuously deflect while propagating along GBs. Additionally, the fracture surface reveals that, in some instances, the crack needs to propagate through the grain interior simply because there is no well-oriented GB nearby, as illustrated by the blue grain in Fig. 6(h). Our recent study found that GBs of hard coatings exhibit considerably lower fracture toughness compared to their single crystalline counter bodies with the identical chemical composition [34]. Furthermore, crack deflection and the necessity of propagating through tougher regions can modify the energy release rate at the tip of a kinked crack [8], potentially impeding crack propagation and thereby increasing fracture toughness.

In contrast, when the crack propagates along well-aligned, elongated GBs—i.e., parallel to the loading direction—it can easily propagate upon nucleation without kinking (Fig. 6(d)). Although no direct evidence of crack branching was observed in the ⊥-notched samples, it can be speculated that this phenomenon is more likely to occur in these ⊥-notched samples than in those with ‖-notches due to the smaller grain size in the crack propagation direction.

To summarize, previous studies have suggested that GB engineering [20,35–38] could be a promising way to strengthen hard coatings, and our findings demonstrate that simply orienting the columnar grained microstructure can improve fracture toughness even without altering their microstructure or composition.

4. Conclusions

Three hard coatings—CrN, AlN and their multilayered variant—all

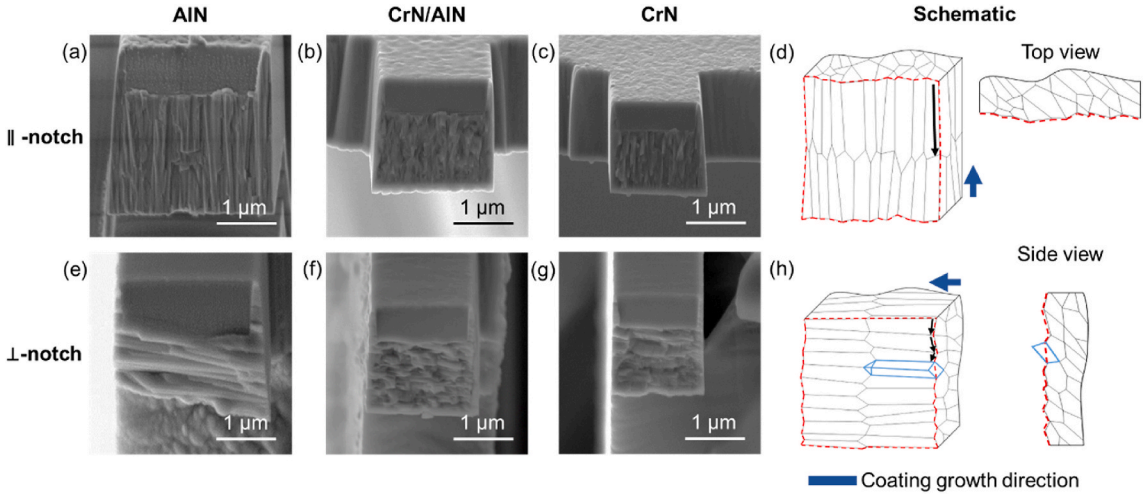

Fig. 6. Fracture surface of AlN, CrN/AlN, and CrN coatings with different notches. (a)–(c) The first row shows surfaces with a ‖-notch, (e)–(g) while the second row shows those with a ⊥-notch. (d) Schematic illustration of crack propagation direction in different geometries with columnar grain structure. The black arrows indicate the direction of crack propagation. The crack propagation is parallel to the growth direction, and in (h) the crack propagation is perpendicular to the growth direction.

exhibiting a columnar grain structure, were deposited using unbalanced reactive magnetron sputtering. Their fracture behavior was quantitatively investigated using *in situ* SEM micro-cantilever bending tests focusing on GB orientation-dependent cracks propagation, i.e. parallel and perpendicular to the elongated grain shape. The results clearly demonstrate that crack deflection along GBs significantly influences fracture toughness. Specifically, when cracks propagate perpendicular to the coating growth direction, the fracture toughness increases by approximately 8 % compared to the parallel case, due to enhanced crack deflection and occasional transgranular fracture. Among the coatings, CrN exhibited the highest fracture toughness, which may be attributed to its relatively uniform cubic structure and favorable residual stress state. The CrN/AlN multilayer also showed toughening effects due to its nanoscale architecture, likely due to increased interface density. These findings highlight the critical role of GB orientation and microstructural design in improving the fracture performance of hard coatings.

CRediT authorship contribution statement

Yinxia Zhang: Writing – original draft, Visualization, Methodology, Investigation, Formal analysis, Data curation. **Matthias Bartosik:** Writing – review & editing, Resources, Methodology. **Steffen Brinckmann:** Writing – review & editing. **Subin Lee:** Writing – review & editing, Supervision, Software, Project administration. **Christoph Kirchlechner:** Writing – review & editing, Supervision, Project administration, Funding acquisition, Conceptualization.

Declaration of competing interest

The authors declare that they have no known competing financial interests or personal relationships that could have appeared to influence the work reported in this paper.

Acknowledgements

The authors acknowledge funding within the framework of the DACH program by the national funding agencies: Austrian Science Fund (FWF) [I4720] and German Research Foundation (DFG) [436506789]. Support from the Helmholtz Program Materials Systems Engineering and the Robert-Bosch-Foundation is gratefully acknowledged. The authors thank M. T. Becker for the support in the film deposition and, the hardness and Young's modulus measurement.

Appendix A. Supplementary data

Supplementary data to this article can be found online at https://doi.org/10.1016/j.msea.2025.148392.

Data availability

Data will be made available on request.

References

[1] P. Visser, H. Terryn, J.M.C. Mol, Aerospace coatings, in: J.M.C.M.A.E. Hughes, M. L. Zheludkevich, R.G. Buchheit (Eds.), Active Protective Coatings, Springer, Dordrecht, 2016, pp. 315–372.
[2] A.M. Merlo, The contribution of surface engineering to the product performance in the automotive industry, Surf. Coat. Technol. 174 (2003) 21–26.
[3] K. Bobzin, High-performance coatings for cutting tools, CIRP J. Manuf. Sci. Technol. 18 (2017) 1–9.
[4] P.H. Mayrhofer, C. Mitterer, L. Hultman, H. Clemens, Microstructural design of hard coatings, Prog. Mater. Sci. 51 (8) (2006) 1032–1114.
[5] N. Schalk, M. Tkadletz, C. Mitterer, Hard coatings for cutting applications: physical vs. chemical vapor deposition and future challenges for the coatings community, Surf. Coat. Technol. 429 (2022) 127949.
[6] M.F. Montemor, Functional and smart coatings for corrosion protection: a review of recent advances, Surf. Coat. Technol. 258 (2014) 17–37.
[7] Z. Gao, J. Buchinger, R. Hahn, Z. Chen, Z.L. Zhang, N. Koutná, P.H. Mayrhofer, Bilayer period and ratio dependent structure and mechanical properties of TiN/MoN superlattices, Acta Mater. 279 (2024) 120313.
[8] T.L. Anderson, Fracture Mechanics: Fundamentals and Applications, third ed., CRC Press, Boca Raton, 2005.
[9] ASTM E399-90, Standard Test Method for plane-strain Fracture Toughness of Metallic Materials, Annual book of ASTM standards, 1997.
[10] J. Ast, M. Ghidelli, K. Durst, M. Göken, M. Sebastiani, A.M. Korsunsky, A review of experimental approaches to fracture toughness evaluation at the micro-scale, Mater. Des. 173 (2019) 107762.
[11] G.R. Irwin, Analysis of stresses and strains near the end of a crack traversing a plate, J. Appl. Mech. 24 (3) (1957) 361–364.
[12] M. Kuczyk, M. Zawischa, T. Krülle, J. Vollhüter, S. Zeiler, M. Leonhardt, J. Kaspar, O. Zimmer, M. Göken, C. Leyens, M. Zimmermann, In situ mechanical testing of hard yet tough high entropy nitride coatings deposited on compliant steel substrates, Thin Solid Films 787 (2023) 140137.
[13] J.A. Stewart, D.E. Spearot, Phase-field simulations of microstructure evolution during physical vapor deposition of single-phase thin films, Comput. Mater. Sci. 131 (2017) 170–177.
[14] J.A. Thornton, High rate thick film growth, Annu. Rev. Mater. Sci. 7 (1) (1977) 239–260.
[15] P. Panjan, M. Čekada, M. Panjan, D. Kek-Merl, Growth defects in PVD hard coatings, Vacuum 84 (1) (2009) 209–214.
[16] F. Konstantiniuk, M. Schiester, M. Tkadletz, C. Czettl, N. Schalk, Annealing activated substrate element diffusion and its influence on the microstructure and mechanical properties of CVD TiN/TiCN coatings, Surf. Coating. Technol. 488 (2024) 131079.
[17] D. Di Maio, S.G. Roberts, Measuring fracture toughness of coatings using focused-ion-beam-machined microbeams, J. Mater. Res. 20 (2) (2005) 299–302.
[18] K. Matoy, H. Schönherr, T. Detzel, T. Schöberl, R. Pippan, C. Motz, G. Dehm, A comparative micro-cantilever study of the mechanical behavior of silicon based passivation films, Thin Solid Films 518 (1) (2009) 247–256.
[19] J.S.-L. Gibson, S. Rezaei, H. Rueß, M. Hans, D. Music, S. Wulfinghoff, J. M. Schneider, S. Reese, S. Korte-Kerzel, From quantum to continuum mechanics: studying the fracture toughness of transition metal nitrides and oxynitrides, Mater. Res. Lett. 6 (2) (2018) 142–151.
[20] R. Daniel, M. Meindlhumer, W. Baumegger, J. Zalesak, B. Sartory, M. Burghammer, C. Mitterer, J. Keckes, Grain boundary design of thin films: using tilted brittle interfaces for multiple crack deflection toughening, Acta Mater. 122 (2017) 130–137.
[21] H. Gopalan, A. Marshal, M. Hans, D. Primetzhofer, N. Cautaerts, B. Breitbach, B. Völker, C. Kirchlechner, J.M. Schneider, G. Dehm, On the interplay between microstructure, residual stress and fracture toughness of (Hf-Nb-Ta-Zr) C multi-metal carbide hard coatings, Mater. Des. 224 (2022) 111323.
[22] B. Völker, B. Stelzer, S. Mráz, H. Rueß, R. Sahu, C. Kirchlechner, G. Dehm, J. M. Schneider, On the fracture behavior of Cr2AlC coatings, Mater. Des. 206 (2021) 109757.
[23] C. Tian, Y. Ma, A. Ghafarollahi, P. Patil, G. Dehm, E. Bitzek, M. Rasinski, J.P. Best, Segregation-enhanced grain boundary embrittlement of recrystallised tungsten evidenced by site-specific microcantilever fracture, Acta Mater. 259 (2023) 119256.
[24] M.R. Schoof, S. Karimi Aghda, C.F. Kusche, M. Hans, J.M. Schneider, S. Korte-Kerzel, J.S.K.L. Gibson, The influence of microstructural orientation on fracture toughness in (V, Al)N and (V, Al)(O, N) coatings as measured by microcantilever bending, J. Mater. Res. 38 (16) (2023) 3950–3965.
[25] R. Daniel, M. Meindlhumer, W. Baumegger, J. Todt, J. Zalesak, T. Ziegelwanger, C. Mitterer, J. Keckes, Anisotropy of fracture toughness in nanostructured ceramics controlled by grain boundary design, Mater. Des. 161 (2019) 80–85.
[26] R. Pippan, A. Hohenwarter, The importance of fracture toughness in ultrafine and nanocrystalline bulk materials, Mater. Res. Lett. 4 (3) (2016) 127–136.
[27] Y. Xiao, Y. Zou, H. Ma, A.S. Sologubenko, X. Maeder, R. Spolenak, J.M. Wheeler, Nanostructured NbMoTaW high entropy alloy thin films: high strength and enhanced fracture toughness, Scr. Mater. 168 (2019) 51–55.
[28] Y. Zhang, M. Bartosik, S. Brinckmann, S. Lee, C. Kirchlechner, Direct observation of crack arrest after bridge notch failure: a strategy to increase statistics and reduce FIB-Artifacts in micro-cantilever testing, Mater. Des. 233 (2023) 112188.
[29] M.-T. Becker, Synthesis and Characterization of B1-AlN Containing Superlattice Structures, Montanuniversitaet Leoben, 2022.
[30] M. Bartosik, D. Holec, D. Apel, M. Klaus, C. Genzel, J. Keckes, M. Arndt, P. Polcik, C.M. Koller, P.H. Mayrhofer, Thermal expansion of Ti-Al-N and Cr-Al-N coatings, Scr. Mater. 127 (2017) 182–185.
[31] W.C. Oliver, G.M. Pharr, An improved technique for determining hardness and elastic modulus using load and displacement sensing indentation experiments, J. Mater. Res. 7 (6) (1992) 1564–1583.
[32] B.N. Jaya, Fracture in small-scale structures and confined volumes, MRS Bull. 47 (8) (2022) 832–838.
[33] B.N. Jaya, C. Kirchlechner, G. Dehm, Can microscale fracture tests provide reliable fracture toughness values? A case study in silicon, J. Mater. Res. 30 (5) (2015) 686–698.
[34] Y. Zhang, M. Bartosik, S. Brinckmann, U. Bansal, S. Lee, C. Kirchlechner, Columnar grain boundaries are the weakest link in hard coatings: insights from micro-cantilever testing with bridge notches, arXiv (2024).
[35] Z. Li, P. Munroe, Z.-t. Jiang, X. Zhao, J. Xu, Z.-f. Zhou, J.-q. Jiang, F. Fang, Z.-h. Xie, Designing superhard, self-toughening CrAlN coatings through grain boundary engineering, Acta Mater. 60 (16) (2012) 5735–5744.

[36] M. Wurmshuber, S. Jakob, S. Doppermann, S. Wurster, R. Bodlos, L. Romaner, V. Maier-Kiener, D. Kiener, Tuning mechanical properties of ultrafine-grained tungsten by manipulating grain boundary chemistry, Acta Mater. 232 (2022) 117939.

[37] X. Min, Y. Kimura, T. Kimura, K. Tsuzaki, Delamination toughening assisted by phosphorus in medium-carbon low-alloy steels with ultrafine elongated grain structures, Mater. Sci. Eng. A 649 (2016) 135–145.

[38] L. Liu, Q. Ruan, Z. Wu, T. Li, W. Zuo, C. Huang, Y. Wu, Z. Wu, R.K. Fu, P.K. Chu, Hard and tough CrN coatings strengthened by high-density distorted coherent grain boundaries, J. Alloy. Compd. 894 (2022) 162139.